Supporting Information

Engineering electronic regulation of ultrafine Ru nanoparticles for boosting hydrogen oxidation and evolution electrocatalysis

Jianling Dong[a], Xiang Ding[a], Luyu Liu[a], Hongli Liu[a], Siyuan Tang[a], Haotian Qin[a], Nan Jiang[b*], Fuzhan Song[a*]

[a] School of Materials Science and Engineering, Jiangsu University, Zhenjiang, Jiangsu 212013, China

[b]Department of Chemistry and Chemical Engineering, Guizhou University, Guiyang, Guizhou 550025, China

1. Characterization

Energy dispersive spectroscopy (EDS) and scanning electron microscopy (SEM) were performed and elemental mapping images were obtained using an JEOL JSM 7800F. The X-ray photoelectron spectroscopy (XPS) measurements were performed using a Kratos Axis Ultra instrument (Kratos Analytical Ltd.). The high-resolution transmission electron microscopy (HRTEM) measurement was carried out on an FEI Tecnai G2 F20 FE-TEM.

2. Syntheses of electrocatalysts

2.1 Syntheses of Cr_2C.

Cr_2C was obtained via an HF-etching method. 2 g of LiF were added to a solution of 30 mL of 9 M HCl, which was then stirred at 550 rpm for 30 minutes. Next, 1 g of Cr_2AlC MAX was added to the solution in an ice bath and stirred for an additional 30 minutes. Following the 24-hour etching process at 40 °C, the solution was centrifuged with DI water at 3500 rpm for 6 minutes, a process that was repeated 6–7 times until the pH reached a neutral state. The Cr_2C precipitate obtained after centrifugation was then stored in a vacuum desiccator for further use.

2.2 Syntheses of CrO_x@Cr_2C.

300 mg of Cr_2C was dispersed in 30 mL ethanol and sonicated at 400 W for 1h. The suspension was transferred into a 40 mL PTFE autoclave for solvothermal treatment at 120 °C for 12 hours. Afterward, the as-prepared suspension was centrifuged at 3500 rpm for 5 min. The obtained solid was freeze-dried and stored in a vacuum desiccator for further use.

2.3 Syntheses of Ru/CrO_x@Cr_2C.

25mg of Cr_2O_3@Cr_2C were added to 25 ml of DI water and subjected to sonication for a period of 30 minutes. Then, 0.02 mmol of a $RuCl_3$ solution was added to the

aforementioned sonicated solution and stirred on a magnetic stirring apparatus at a speed of 550 rpm for a period of 30 minutes. 35 mg of $NaBH_4$ was mixed with 1 ml of DI water that was added rapidly to solution. Following the addition of the $NaBH_4$, which was stirred at 750 rpm for five minutes and then at 550 rpm for 30 minutes, the solution was centrifuged with deionized water three times at 6000 rpm for three minutes. The resulting material is $Ru/CrO_x@Cr_2C$ and was subsequently placed in a vacuum desiccator.

3. Electrochemical measurement

The catalysts was prepared by ultrasonically mixing 4 mg of the catalyst powder in a mixture consisting of 1160 μL of ethanol, 800 μL of H_2O, and 40 μL of a 5% Nafion solution for 1 h, this produced homogeneous catalyst inks having densities of 2 mg/mL. Next, 20 or 160 μL of the catalyst ink was carefully dropped onto a polished glassy carbon rotating disk electrode (RDE, 0.19625 cm^2) or onto carbon paper (CP, 0.25 cm^2), respectively. The corresponding Ru loading on electrodes are 0.066 mg/cm^2 ($Ru/CrO_x@Cr_2C$) and 0.067 mg/cm^2 (Ru/Cr_2C) for HER electrode on CP and 0.011 mg/cm^2 ($Ru/CrO_x@Cr_2C$) and 0.011 mg/cm^2 (Ru/Cr_2C) for HOR electrode on RDE.

Pt loading on CP is 0.128 mg/cm^2.

All electrochemical experiments were performed using a VSP-300 Multichannel Electrochemical Workstation with a three-electrode configuration. The current densities in this work were calculated on the basis of the geometric area of each working electrode. The monolithic $Ru/CrO_x@Cr_2C$ composite supported on CP, with a loading of 0.066 mg cm^{-2}, was directly used as the working electrode. A calibrated Hg/HgCl (saturated KCl) with a salt bridge kit and a carbon rod were used as the counter and

reference electrode, respectively. The electrolyte for HER was 1.0 M KOH. While for HOR, the Ru/CrO_x@Cr_2C supported on RDE was used as the working electrode in a 0.1 M KOH electrolyte. H_2 was bubbled through all electrolytes used during each electrochemical experiment. All potentials are reported versus reversible hydrogen electrode (RHE) according to the following equation:

$$E\ (vs.\ RHE) = E\ (vs.\ Hg/HgCl) + 0.241 + 0.059 \times pH \qquad (S1)$$

Linear sweep voltammetry (LSV)

All polarization curves were recorded using linear scan voltammetry (LSV). The scan rate was 5 mV/s for HER and 1 mV/s for HOR. Unless otherwise stated, all LSV curves for HER were iR corrected and obtained by scanning from a negative to positive potential. A correction was made according to the following equation:

$$E_{corrected} = E_{measured} - iR_s \qquad (S2)$$

where $E_{corrected}$ is the iR-corrected potential, $E_{measured}$ and i are experimentally measured potential and current, respectively, and R_s is the equivalent series resistance measured via electrochemical impedance spectroscopy. Tafel plots were constructed using the equation:

$$\eta = a + b\log|j| \qquad (S3)$$

where η is the overpotential, a is the intercept, b is the Tafel slope, and j is the current density.

Electrochemical impedance spectroscopy (EIS)

Electrochemical impedance spectroscopy (EIS) measurements in 1.0 M KOH were carried out at -0.04 V vs RHE in the frequency range of 10^6 – 0.01 Hz.

Electrochemically active surface area (ECSA)

The electrochemically active surface area (ECSA) of each working electrode was determined according to an established methodology reported in the literature. CV cycling was repeated using a range of scan rates from 20 to 100 mV s^{-1}. The electrochemical double-layer capacitance (C_{dl}) was then estimated by plotting the difference between the anodic and cathodic current densities ($\Delta j = j_a - j_c$) at OCP against the scan rate. The resulting linear slope is twice of the C_{dl}. The ESCA can be calculated according to the following equation: $ECSA = C_{dl}/C_s$, where Cs is the specific capacitance of a flat smooth surface of the electrode material, according to the literature.

Chronopotentiometry (CP)

The catalytic stability for HER was evaluated by either chronopotentiometry (CP) measurements without iR correction and temperature-controlled system. For HER, CP was measured at a current density of -10 and -100 $mAcm^{-2}$ in 1.0 M KOH solution.

Mass-specific current

The mass activity was defined as the current at potential of 100 mV vs RHE for HER and 50 mV vs RHE for HOR normalized by the mass of the catalyst loaded on the electrode. The mass-specific current was calculated by application of equation:

$$i_{mass} = i/m_{catalyst} \qquad (S4)$$

where i_{mass} represents the mass activity; i is the electrochemically measured current at

potential of 100 mV vs RHE for HER and 50 mV vs RHE for HOR; m_{catalyst} is the mass of the catalyst loaded on the working electrode, which was confirmed by ICP results.

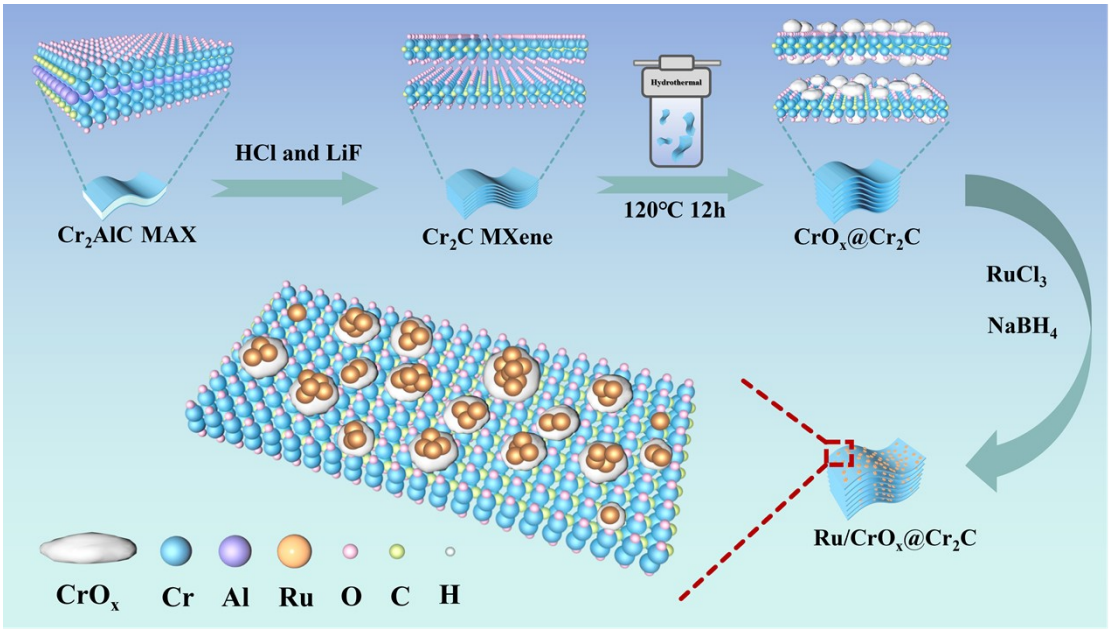

Fig. S 1 Schematic illustration of facile synthesis of $Ru/CrO_x@Cr_2C$ from Cr_2AlC (MAX).

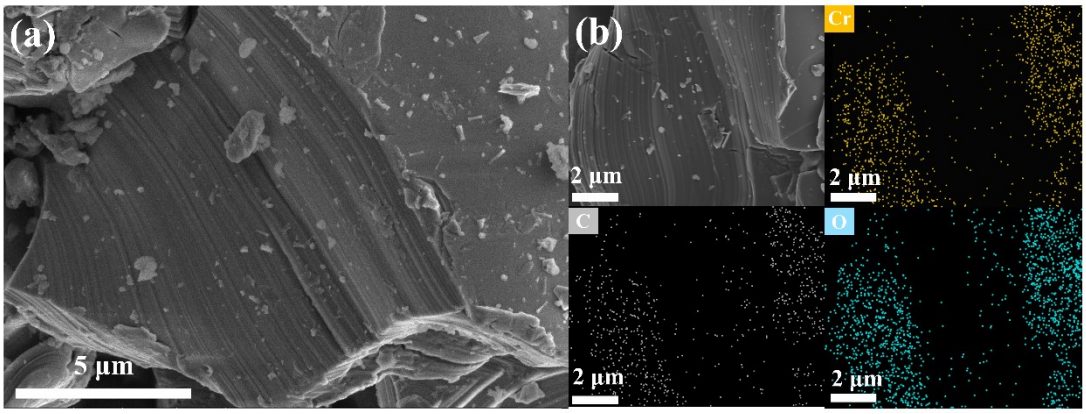

Fig. S2 (a) SEM image of Cr_2C MXene. (b) SEM-EDX mappings of Cr, C and O elements.

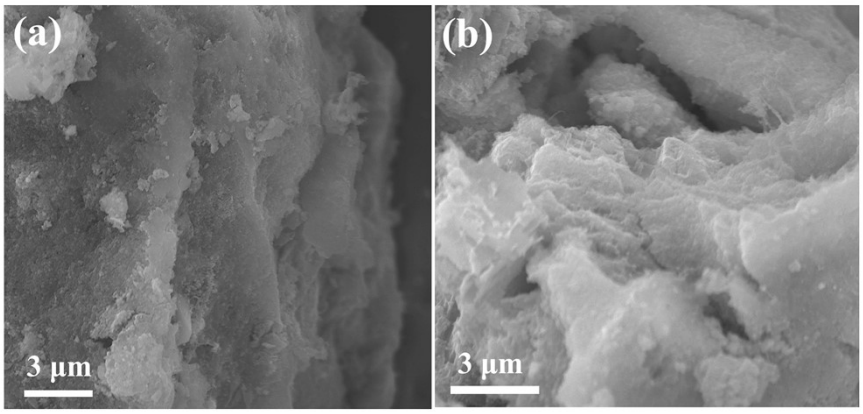

Fig. S3 (a,b) SEM image of CrO_x@Cr_2C.

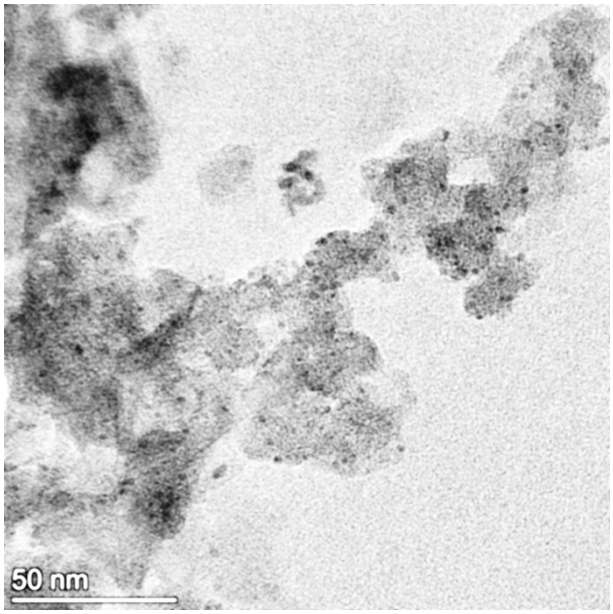

Fig. S4 TEM image of $Ru/CrO_x@Cr_2C$.

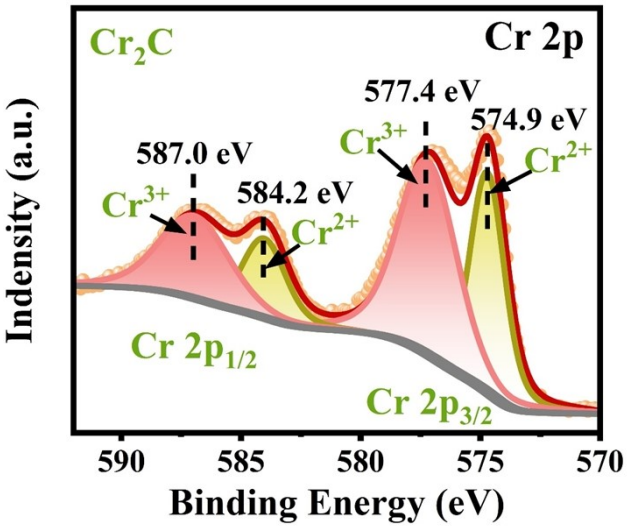

Fig. S5 High-resolution Cr 2p XPS spectra of Cr_2C.

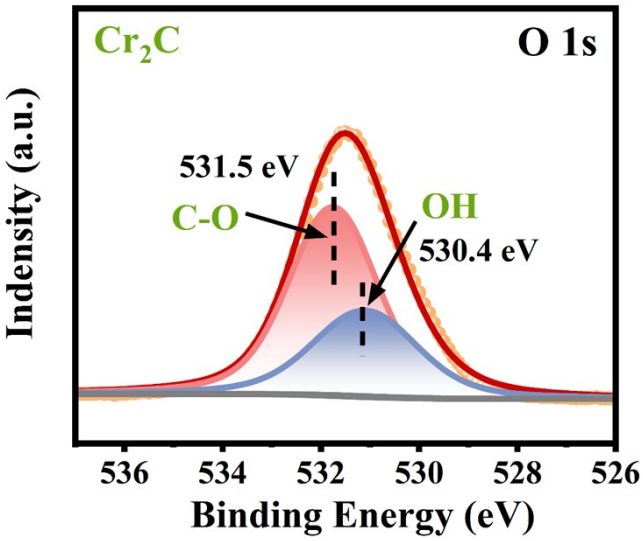

Fig. S6 High-resolution O 1s XPS spectra of Cr_2C.

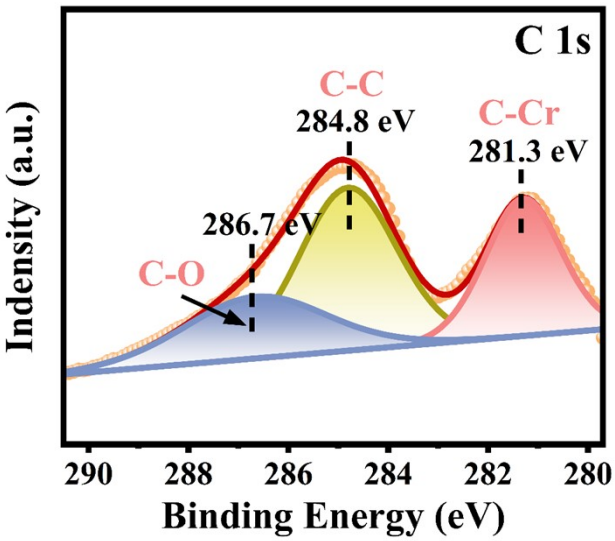

Fig. S7 High-resolution XPS spectra of $Ru/CrO_x@Cr_2C$: C 1s.

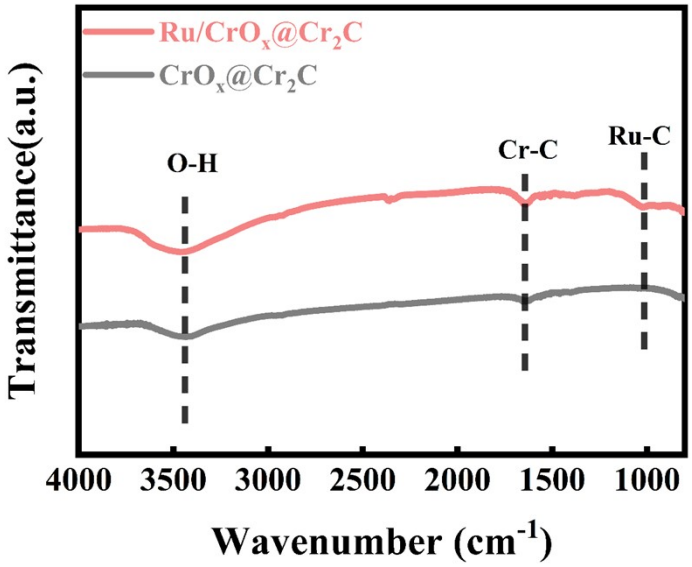

Fig. S8 Fourier transform infrared (FT-IR) spectra of Ru/CrO_x@Cr_2C and CrO_x@Cr_2C.

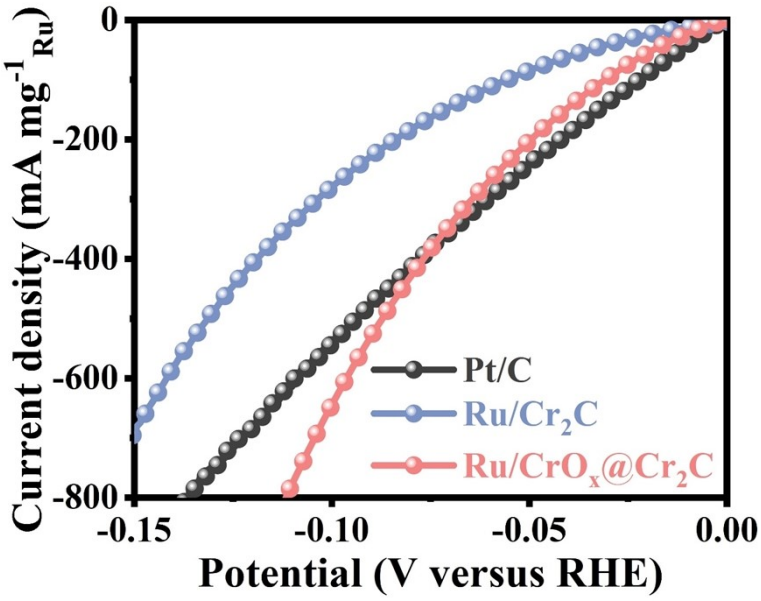

Fig. S9 HER LSVs normalized by metal loading mass for Ru/Cr_2C, Pt/C and $Ru/CrO_x@Cr_2C$ catalysts in 1.0 M KOH.

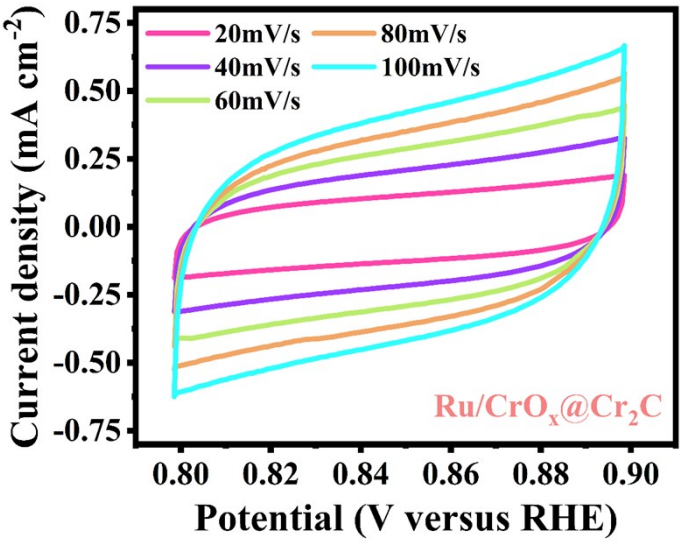

Fig. S10 CV of Ru/CrO_x@Cr_2C recorded from 0.79 to 0.89 V at different rates from 20 to 100 mV s^{-1}.

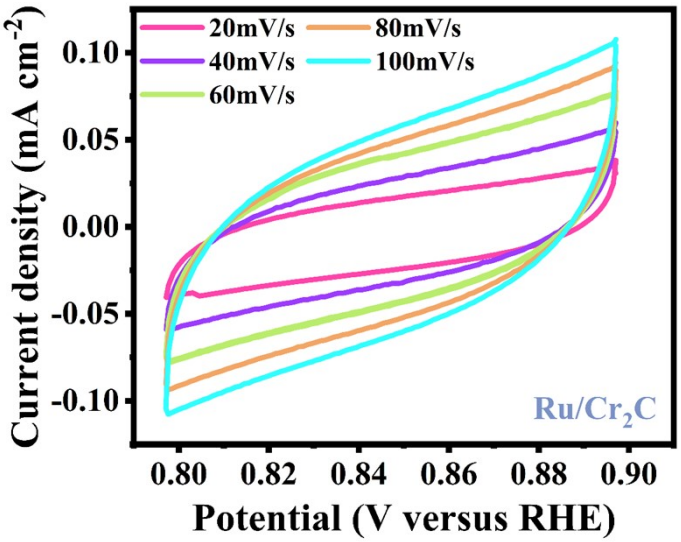

Fig. S11 CV of Ru/Cr_2C recorded from 0.79 to 0.89 V at different rates from 20 to100 mV s^{-1}.

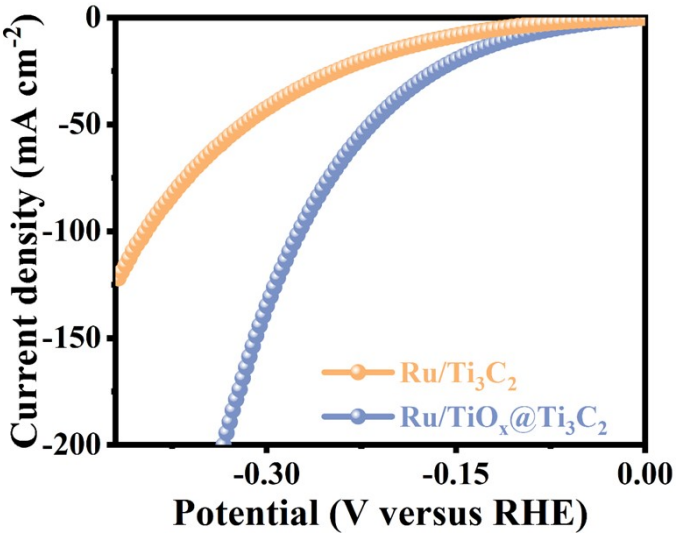

Fig. S12 LSV curves of Ru/Ti_3C_2 and $Ru/TiO_x@Ti_3C_2$ in 1.0 M KOH.

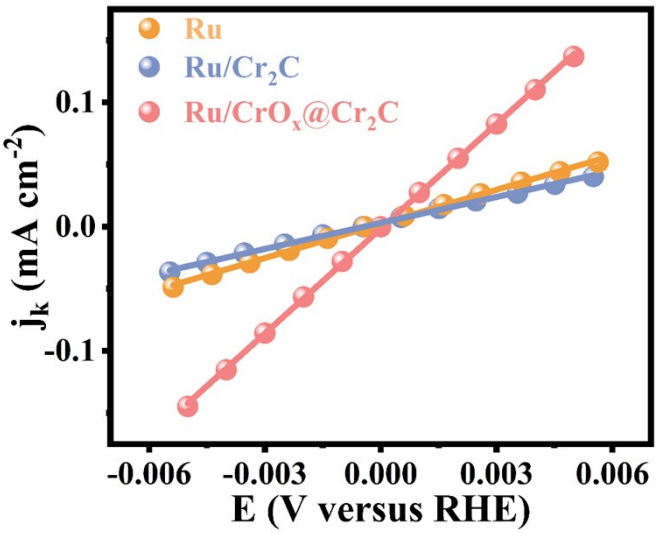

Fig. S13 micro-polarization region. The solid lines signify the linear fitting of the data.

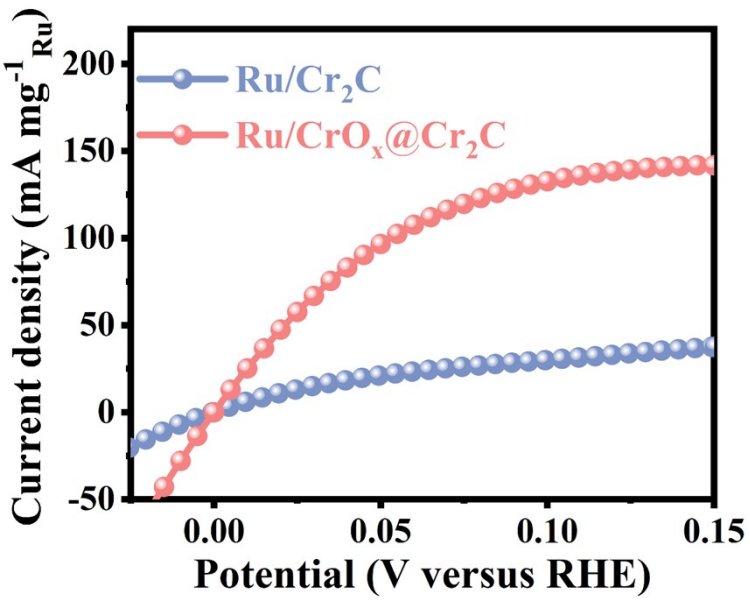

Fig. S14 HOR LSVs normalized by Ru loading mass for Ru/Cr_2C and Ru/CrO_x@Cr_2C catalysts in 1.0 M KOH.

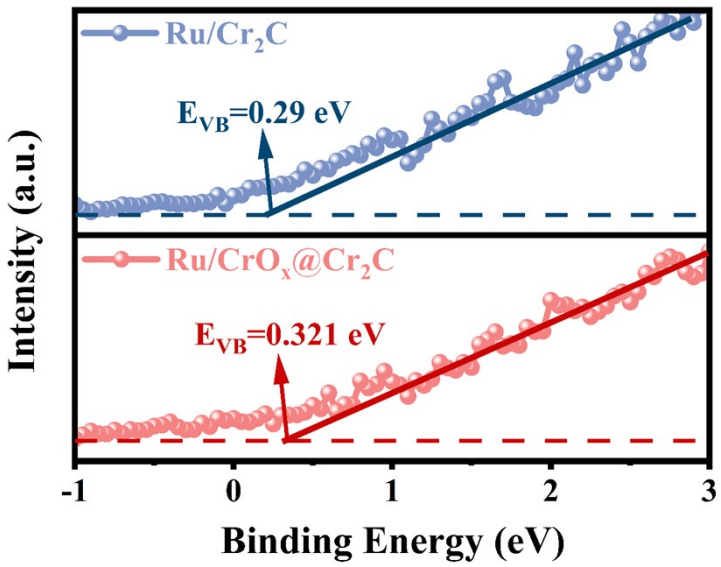

Fig. S15 UPS spectrum obtained valence band edge of Ru/Cr_2C and $Ru/CrO_x@Cr_2C$.

Tauc's empirical formula was employed to determine the optical bandgap of the samples, as expressed by the equation:[1, 2]

$$(\alpha hv)^2 = A(hv - E_g) \#(S5)$$

Here, hv denotes the photon energy, A is a constant, and E_g represents the bandgap energy.

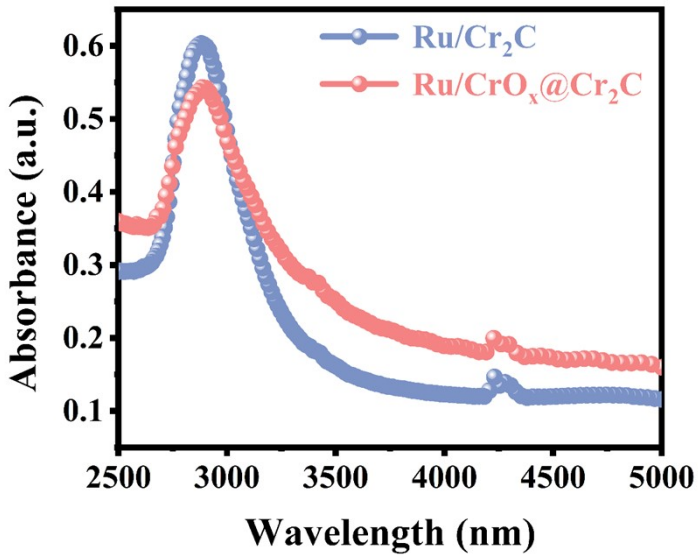

Fig. S16 FTIR absorption spectra of Ru/Cr_2C and $Ru/CrO_x@Cr_2C$.

FTIR absorption spectra reveals that $Ru/CrO_x@Cr_2C$ exhibits a stronger absorption in the 2500–3500 nm region relative to Ru/Cr_2C, which can be ascribed to the modified surface chemical environment induced by the in-situ grown CrO_x species, implying the formation of specific interactions between CrO_x and the substrate.

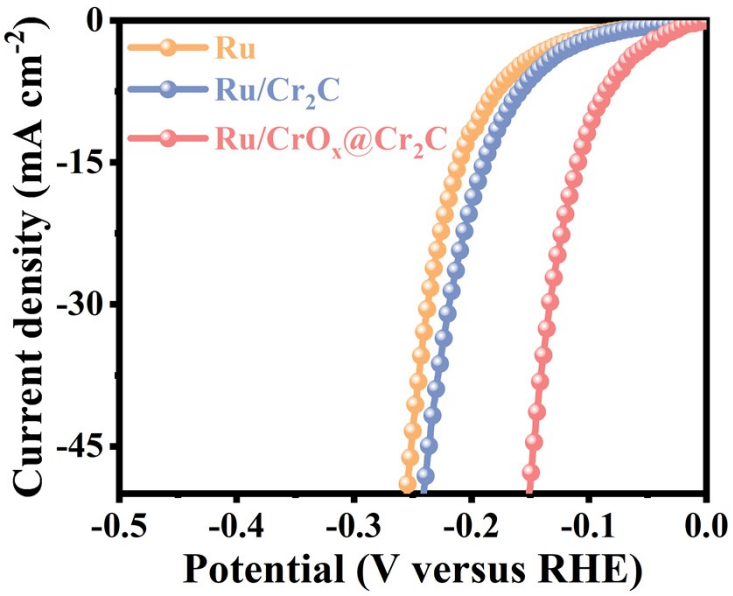

Fig. S17 LSV curves of Ru, Ru/Cr_2C and $Ru/CrO_x@Cr_2C$ in 0.5 M H_2SO_4.

Table S 1 Comparisons of the Tafel slopes and overpotentials at the current density of 10 mA cm^{-2} of reported catalysts for HER in 1 M KOH solution.

Catalysts	η_{10} (mV)	Tafel slope (mV/dec)	Ref.
Ru/CrO_x@Cr_2C	40.5	29	This work
Ru-Ni@Ni_2P-NRs	31	41	[3]
Ru@CN	32	53	[4]
Ni_5P_4-Ru	54	52	[5]
Ru/CeO_2	47	41	[6]
Ru-MoO_2	55	44	[7]
Ru@NG-4[b]	60	41	[8]
Ru-HPC	61.6	66.8	[9]
Ru-GC (Ru-MeOH/THF)	83	46	[10]
Ru-GC	90	33	[11]
s-RuS_2/S-rGO	69	64	[12]
Ru/TiON-C	42	40	[13]
0.5Metallic Ru.1Cu-GN1000	68	54	[14]
Ru-C_3N_4/rGO	80	55	[15]
Atomically dispersed Ni-Ru-P	57	75	[16]
Ru-CoO@SNG	90	77	[17]
Ru/C-TiO_2	44	73.7	[18]
Ru–Cr_2O_3/NG	47	39	[19]
Ru@Co/N-CNT	48	33	[20]

Supplementary Table 2. Comparison of the HOR performance for $Ru/CrO_x@Cr_2C$ with the recently reported noble metal-based electrocatalysts in 0.1M KOH.

Catalysts	j_0 (mA cm^{-2})	$j_{k,m}$@50mV (mA/mg_{PGM})	Ref.
$Ru/CrO_x@Cr_2C$	1.404	77.8	This work
PtRu/C	/	80	[21]
IrNi@Ir/C	1.22	1.12	[22]
hcp RuNi	1.98	82	[23]
RuRh/Co	1.91	11	[24]
D-IrFe/C	/	80	[25]
Ru nanoassembly	/	41	[26]
Ru/C	/	52	[27]
Ru/RuO_2-180	/	~24	[28]
Ru SA/NC	/	14.56	[29]
Pd $(OH)_2$ (1:1)	0.075	95	[30]
$Ru/Ru_xFe_{3-x}O_4$	2.92	61	[31]
$RuP@RuP_2/C$	/	25 mV@45	[32]
Ru/C-H_2O/CH_3CH_2OH	/	41.1	[26]
Ru/C-H_2O	/	3.56	[26]
PtRu NWs	/	0.6	[33]

References

[1] H. Dong, Y. Gao, X. Zhang, Z. Li, W. Feng, In-situ oxygen sensitizing PbSnSe films for high-performance photoelectronic detection, Beijing Key Laboratory of Special Elastomer Composite Materials, College of New Materials and Chemical Engineering, Beijing Institute of Petrochemical Technology, Beijing, 102617, China, Vol.207 (2023) 111538.

[2] H. Yang, G. Wang, X. Li, J. Zheng, Effect of in situ O+ beam induction on the microstructures and optical properties of polycrystalline lead selenide films, MOE Key Laboratory of Material Physics and Chemistry under Extraordinary Conditions and Shaanxi Key Laboratory of Optical Information Technology, School of Science, Northwestern Polytechnical University, Xi'an 710072, China, Vol.251 (2019) 85-88.

[3] Y. Liu, S.L. Liu, Y. Wang, Q.H. Zhang, L. Gu, S.C. Zhao, D.D. Xu, Y.F. Li, J.C. Bao, Z.H. Dai, Ru Modulation Effects in the Synthesis of Unique Rod-like Ni@Ni_2P-Ru Heterostructures and Their Remarkable Electrocatalytic Hydrogen Evolution Performance, J. Am. Chem. Soc., 140 (2018) 2731-2734.

[4] J. Wang, Z.Z. Wei, S.J. Mao, H.R. Li, Y. Wang, Highly uniform Ru nanoparticles over N-doped carbon: pH and temperature-universal hydrogen release from water reduction, Energy Environ. Sci., 11 (2018) 800-806.

[5] Q. He, D. Tian, H.L. Jiang, D.F. Cao, S.Q. Wei, D.B. Liu, P. Song, Y. Lin, L. Song, Achieving Efficient Alkaline Hydrogen Evolution Reaction over a Ni5P4 Catalyst Incorporating Single-Atomic Ru Sites, Adv. Mater., 32 (2020) 8.

[6] E. Demir, S. Akbayrak, A.M. Önal, S. Özkar, Nanoceria-Supported Ruthenium(0) Nanoparticles: Highly Active and Stable Catalysts for Hydrogen Evolution from Water, ACS Appl. Mater. Interfaces, 10 (2018) 6299-6308.

[7] P. Jiang, Y. Yang, R.H. Shi, G.L. Xia, J.T. Chen, J.W. Su, Q.W. Chen, Pt-like electrocatalytic behavior of Ru-MoO_2 nanocomposites for the hydrogen evolution reaction, J. Mater. Chem. A, 5 (2017) 5475-5485.

[8] B.K. Barman, D. Das, K.K. Nanda, Facile synthesis of ultrafine Ru nanocrystal supported N-doped graphene as an exceptional hydrogen evolution electrocatalyst in both alkaline and acidic media, Sustain. Energ. Fuels, 1 (2017) 1028-1033.

[9] T.J. Qiu, Z.B. Liang, W.H. Guo, S. Gao, C. Qu, H. Tabassum, H. Zhang, B.J. Zhu, R.Q. Zou, Y. Shao-Horn, Highly exposed ruthenium-based electrocatalysts from bimetallic metal-organic frameworks for overall water splitting, Nano Energy, 58 (2019) 1-10.

[10] S. Drouet, J. Creus, V. Collière, C. Amiens, J. García-Antón, X. Sala, K. Philippot, A porous Ru nanomaterial as an efficient electrocatalyst for the hydrogen evolution reaction under acidic and neutral conditions, Chem. Commun., 53 (2017) 11713-11716.

[11] K. Magdic, K. Kvastek, V. Horvat-Radosevic, Impedance approach to activity of hydrogen evolution reaction on spatially heterogeneous GC electrode surfaces: metal free vs. Ru catalysed case, Electrochim. Acta, 167 (2015) 455-469.

[12] J. Yu, Y.A. Guo, S.S. Miao, M. Ni, W. Zhou, Z.P. Shao, Spherical Ruthenium Disulfide-Sulfur-Doped Graphene Composite as an Efficient Hydrogen Evolution Electrocatalyst, ACS Appl. Mater. Interfaces, 10 (2018) 34098-34107.

[13] M. Smiljanić, M. Bele, L. Pavko, A. Hrnjić, F. Ruiz-Zepeda, L. Bijelić, A.R. Kamšek, M.

Nuhanović, A. Marsel, L. Gašparič, A. Kokalj, N. Hodnik, Titanium oxynitride-supported Ru nanoparticles as exceptional electrocatalysts for alkaline hydrogen evolution reaction, Chemical Engineering Journal, 517 (2025).
[14] Y.C. Liu, H.T. Huang, X.D. Ding, B.B. Huang, Z.L. Xie, Boosting the HER electrocatalytic activity over RuCu-supported carbon nanosheets as efficient pH-independent catalysts, FlatChem, 30 (2021) 7.
[15] Y. Peng, W.Z. Pan, N. Wang, J.E. Lu, S.W. Chen, Ruthenium Ion-Complexed Graphitic Carbon Nitride Nanosheets Supported on Reduced Graphene Oxide as High-Performance Catalysts for Electrochemical Hydrogen Evolution, ChemSusChem, 11 (2018) 130-136.
[16] K.L. Wu, K.A. Sun, S.J. Liu, W.C. Cheong, Z. Chen, C. Zhang, Y. Pan, Y.S. Cheng, Z.W. Zhuang, X.W. Wei, Y. Wang, L.R. Zheng, Q.H. Zhang, D.S. Wang, Q. Peng, C. Chen, Y.D. Li, Atomically dispersed Ni-Ru-P interface sites for high-efficiency pH-universal electrocatalysis of hydrogen evolution, Nano Energy, 80 (2021) 11.
[17] W. Naseeb, Q.M. Liu, F. Nichols, D.J. Pan, M.K. Khosa, S.W. Chen, Ru-CoO heterostructured nanoparticles supported on nitrogen and sulfur codoped graphene nanosheets as effective electrocatalysts for hydrogen evolution reaction in alkaline media, J. Electroanal. Chem., 932 (2023) 7.
[18] Y.J. Wang, Q.X. Zhu, T.P. Xie, Y. Peng, S.L. Liu, J.K. Wang, Promoted Alkaline Hydrogen Evolution Reaction Performance of Ru/C by Introducing TiO_2 Nanoparticles, ChemElectroChem, 7 (2020) 1182-1186.
[19] L. Tang, J.J. Yu, Y. Zhang, Z.Z. Tang, Y. Qin, Boosting the hydrogen evolution reaction activity of Ru in alkaline and neutral media by accelerating water dissociation, RSC Adv., 11 (2021) 6107-6113.
[20] Z. Liu, X.D. Yang, G.Z. Hu, L.G. Feng, Ru Nanoclusters Coupled on Co/N-Doped Carbon Nanotubes Efficiently Catalyzed the Hydrogen Evolution Reaction, ACS Sustain. Chem. Eng., 8 (2020) 9136-9144.
[21] E.R. Hamo, R.K. Singh, J.C. Douglin, S. Chen, M.B. Hassine, E. Carbo-Argibay, S. Lu, H. Wang, P.J. Ferreira, B.A. Rosen, D.R. Dekel, Carbide-Supported PtRu Catalysts for Hydrogen Oxidation Reaction in Alkaline Electrolyte, ACS Catalysis, 11 (2021) 932-947.
[22] D. Liu, S. Lu, Y. Xue, Z. Guan, J. Fang, W. Zhu, Z. Zhuang, One-pot synthesis of IrNi@Ir core-shell nanoparticles as highly active hydrogen oxidation reaction electrocatalyst in alkaline electrolyte, Nano Energy, 59 (2019) 26-32.
[23] M.M. Fang, Y.J. Ji, S.Z. Geng, J.Q. Su, Y.Y. Li, Q. Shao, J.M. Lu, Metastable Metal-Alloy Interface in RuNi Nanoplates Boosts Highly Efficient Hydrogen Electrocatalysis, ACS Appl. Nano Mater., 5 (2022) 17496-17502.
[24] Y.J. Cui, Z.H. Xu, D. Chen, T.T. Li, H. Yang, X.Q. Mu, X.Y. Gu, H. Zhou, S.L. Liu, S.C. Mu, Trace oxophilic metal induced surface reconstruction at buried RuRh cluster interfaces possesses extremely fast hydrogen redox kinetics, Nano Energy, 90 (2021) 8.
[25] J.X. Jiang, J.H. Liao, S.C. Tao, T. Najam, W. Ding, H.J. Wang, Z.D. Wei, Modulation of iridium-based catalyst by a trace of transition metals for hydrogen oxidation/evolution reaction in alkaline, Electrochim. Acta, 333 (2020) 7.
[26] Y.Z. Li, J. Abbott, Y.C. Sun, J.M. Sun, Y.C. Du, X.J. Han, G. Wu, P. Xu, Ru nanoassembly catalysts for hydrogen evolution and oxidation reactions in electrolytes at various pH values,

Appl. Catal. B-Environ., 258 (2019) 8.
[27] J.X. Jiang, S.C. Tao, Q. He, J. Wang, Y.Y. Zhou, Z.Y. Xie, W. Ding, Z.D. Wei, Interphase-oxidized ruthenium metal with half-filled d-orbitals for hydrogen oxidation in an alkaline solution, J. Mater. Chem. A, 8 (2020) 10168-10174.
[28] X.B. Zhang, L.X. Xia, G.Q. Zhao, B.X. Zhang, Y.P. Chen, J. Chen, M.X. Gao, Y.Z. Jiang, Y.F. Liu, H.G. Pan, W.P. Sun, Fast and Durable Alkaline Hydrogen Oxidation Reaction at the Electron-Deficient Ruthenium-Ruthenium Oxide Interface, Adv. Mater., 35 (2023) 10.
[29] J. Park, H. Kim, S. Kim, S.Y. Yi, H. Min, D. Choi, S. Lee, J. Kim, J. Lee, Boosting Alkaline Hydrogen Oxidation Activity of Ru Single-Atom Through Promoting Hydroxyl Adsorption on Ru/WC_{1-x} Interfaces, Adv. Mater., 36 (2024) 9.
[30] Y.W. Zhao, G.W. Wang, L. Xiao, J.T. Lu, L. Zhuang, Hydrogen Oxidation Reaction on Pd-$Ni(OH)_2$Composite Electrocatalysts in an Alkaline Electrolyte, ChemistrySelect, 5 (2020) 7803-7807.
[31] X.Q. Mu, X.Y. Zhang, Z.Y. Chen, Y. Gao, M. Yu, D. Chen, H.Z. Pan, S.L. Liu, D.S. Wang, S.C. Mu, Constructing Symmetry-Mismatched Ru x Fe3-x O4 Heterointerface-Supported Ru Clusters for Efficient Hydrogen Evolution and Oxidation Reactions, Nano Lett., 24 (2024) 1015-1023.
[32] H.F. Du, Z.Z. Du, T.F. Wang, B.X. Li, S. He, K. Wang, L.H. Xie, W. Ai, W. Huang, Unlocking Interfacial Electron Transfer of Ruthenium Phosphides by Homologous Core-Shell Design toward Efficient Hydrogen Evolution and Oxidation, Adv. Mater., 34 (2022) 9.
[33] M.E. Scofield, Y.C. Zhou, S.Y. Yue, L. Wang, D. Su, X. Tong, M.B. Vukmirovic, R.R. Adzic, S.S. Wong, Role of Chemical Composition in the Enhanced Catalytic Activity of Pt-Based Alloyed Ultrathin Nanowires for the Hydrogen Oxidation Reaction under Alkaline Conditions, Acs Catalysis, 6 (2016) 3895-3908.